Accepted Manuscript

A novel dual-ratiometric-response fluorescent probe for SO_2/ClO^- detection in cells and in vivo and its application in exploring the dichotomous role of SO_2 under the ClO^- induced oxidative stress

Kun Dou, Qiang Fu, Guang Chen, Fabiao Yu, Yuxia Liu, Ziping Cao, Guoliang Li, Xianen Zhao, Lian Xia, Lingxin Chen, Hua Wang, Jinmao You

PII: S0142-9612(17)30254-5

DOI: 10.1016/j.biomaterials.2017.04.024

Reference: JBMT 18044

To appear in: *Biomaterials*

Received Date: 23 January 2017

Revised Date: 23 March 2017

Accepted Date: 13 April 2017

Please cite this article as: Dou K, Fu Q, Chen G, Yu F, Liu Y, Cao Z, Li G, Zhao X, Xia L, Chen L, Wang H, You J, A novel dual-ratiometric-response fluorescent probe for SO_2/ClO^- detection in cells and in vivo and its application in exploring the dichotomous role of SO_2 under the ClO^- induced oxidative stress, *Biomaterials* (2017), doi: 10.1016/j.biomaterials.2017.04.024.

A novel dual-ratiometric-response fluorescent probe for SO_2/ClO^- detection in cells and in vivo and its application in exploring the dichotomous role of SO_2 under the ClO^- induced oxidative stress

Kun Dou[a], Qiang Fu[a], Guang Chen[a,b*], Fabiao Yu[c], Yuxia Liu[a], Ziping Cao[a], Guoliang Li[a], Xianen Zhao[a], Lian Xia[a], Lingxin Chen[c], Hua Wang[a] and Jinmao You[a*]

[a.] *The Key Laboratory of Life-Organic Analysis; Key Laboratory of Pharmaceutical Intermediates and Analysis of Natural Medicine, Qufu Normal University, Qufu 273165, Shandong, China. Corresponding: chenandguang@163.com; jmyou6304@163.com*

[b.] *Chemical Engineering and Materials Science, Engineering Research Center of Pesticide and Medicine Intermediate Clean Production, College of Chemistry, Ministry of Education, Shandong Normal University, Jinan 250014*

[c.] *Key Laboratory of Coastal Environmental Processes and Ecological Remediation, The Research Centre for Coastal Environmental Engineering and Technology, Yantai Institute of Coastal Zone Research, Chinese Academy of Sciences, Yantai 264003, China*

Abstract

Intracellular reactive sulfur species and reactive oxygen species play vital roles in immunologic mechanism. As an emerging signal transmitter, SO_2 can be generated as the anti-oxidant, while SO_2 is also a potential oxidative stress-inducer in organism. Aiming to elucidate in-depth the dichotomous role of SO_2 under oxidative stress, we designed a dual-response fluorescent probe that enabled the respective or successive detection of SO_2 and ClO^-. The probe itself emits the red fluorescence (625 nm) which can largely switch to blue (410 nm) and green fluorescence (500 nm) respectively in response to SO_2 and ClO^-, allowing the highly selective and accurate ratiometric quantification for both SO_2 and ClO^- in cells. Moreover the ultrafast (SO_2: < 60 seconds; ClO^-: within sec) and highly sensitive (detection limits: SO_2: 3.5 nM; ClO^-: 12.5 nM) detection were achieved. With the robust applicability, the developed probe was successfully used to quantify SO_2 and endogenous ClO^- in respectively the HeLa cells and the RAW 264.7 cells, as well as to visualize the dynamic of SO_2/ClO^- in zebrafish. The fluorescent imaging studies and flow cytometry analysis confirmed the burst-and-depletion and meanwhile the oxidative-and-antioxidative effects of intracellular SO_2 under the NaClO induced oxidative stress.

Keywords

Dual-response; dual-ratiometric; quantification; SO_2/ClO^-; Imaging analysis.

1. Introduction

Reactive oxygen species (ROS) and reactive sulfur species (RSS) play the vital role in living body. These species are widely implicated in cell proliferation, cytoprotection and signal transduction[1, 2]. Oxidative stress, due to the overproduction of ROS or the failure in intracellular defenses against ROS, will result in pathogenesis, such as cardiovascular diseases, neurological disorders and even carcinogenesis[3-5]. While, as the natural defense to oxidative stress, organism has built up immunologic mechanism with antioxidant agents that was generated with the aid of enzymes, such as superoxide dismutase, catalase, glutathione peroxidase[6]. Therefore, the interrelation between oxidative-stress with the antioxidant capacity is of great significance to organism. As an emerging signal transmitter, sulfur dioxide (SO_2) can be produced via the oxidation of hydrogen sulfide or sulphur-containing amino acids, and the decomposition of sulfinylpyruvate[7], existing in organism with the form of HSO_3^-. Increasing evidence suggests that SO_2 plays essential roles in regulating the redox status as an antioxidant [8-10]. Therefore, SO_2 should be a non-negligible participant involved in the redox homeostasis against ROS. However, the further bio-function of SO_2 in biological systems still remain largely unknown. On the other hand, a notorious ROS hypochlorous acid (ClO^-), is produced from the myeloperoxidase (MPO)-catalyzed reaction of hydrogen peroxide with chloride ion[3, 11]. As the diffusible oxidant and chlorinating agent, excessive amounts of ClO^- can cause the elevated levels of intracellular chlorotyrosine residues[12, 13] and hypochlorous acid-modified proteins[14], which contributes to the neutrophil-induced cell killing[15]. In the light of the respective oxidative and anti-oxidative property of ClO^- and SO_2, we hypothesize that the intracellular redox state may have the closed correlation with SO_2/ClO^-. However, homeostasis of SO_2/ClO^- in cell or in vivo

has not been reported to the best of our knowledge. In addition, SO_2 is not only the anti-oxidant but also have the potential oxidative ability, thus it will act as both the signaling molecule and the stress-inducer[16, 17]. Therefore, monitoring the cross-talk influence of SO_2/ClO^- to cells should be very significant for understanding the dichotomous role of intracellular SO_2. Unfortunately, no report yet describing the investigation of intracellular SO_2 under the NaClO induced oxidative stress can be found by us.

Owing to their important biological functions, we think, it is necessary to explore in detail the SO_2/ClO^- in cells and in vivo. The main challenge to perform such a study lies in that it is almost impossible to immediately separate SO_2 and ClO^- from biological systems when performing the real time intracellular or in vivo monitoring. In such a case, a dual-response probe is much needed, because it can selectively report the two analytes. Moreover, the dual-response can avoid the interference of photo-bleaching and spectral overlap, as well as the uneven probe loading and nonhomogeneous distribution[18]. The other challenge lies in that biological signaling molecules are always produced in the trace level. Therefore, this dual-response probe should be highly sensitive and ultrafast, so that to follow the analytes in time. Another challenge lies in that, during the NaClO induced oxidative stress, the fall-and-rise of SO_2 and ClO^- in the dynamic equilibrium need to be selectively and continuously monitored. Thus, the desired probe should also have the ability to respond to SO_2 and ClO^- successively, otherwise, some information about the combined effect of SO_2 and ClO^- on cells would be missed. Consequently, we need a dual-response (preferably continuous-response) probe that can selectively, sensitively and rapidly report SO_2 and ClO^- in cells or in vivo. With these issues and plans in mind, we conducted the literature research. Traditional methods including chromatography[19], electrochemistry[20], and ion chromatograph[21]have been used to perform the in vitro study.

Obviously, these technologies are not suitable for the real-time analysis of SO_2/endogenous ClO^- in cell and in vivo. In contrast, fluorescence imaging technique with the aid of a probe possesses unique advantage in terms of specific recognition, non-separation, real-time monitoring, less invasion, convenient operation and analytical visualization, making this technique a more attractive alternative to the traditional technologies for biological monitoring[22-27]. To date, many excellent probes have been elaborated for the respective detection of SO_2 and NaClO [28-30]. Unfortunately, no dual-response fluorescent probe for SO_2/ClO^- detection was found by us, which highlighted the significance of designing a sensitive and rapid continuous dual-response SO_2/ClO^- probe and its application in cells and in vivo.

Herein, we designed a novel dual-response fluorescent probe 2-(4-(1-methyl-phenanthro-9,10-imidazole-2-yl)-benzylidene) malononitrile (MPIBA) consisting of a phenanthroimidazole-modified fluorophore and a malononitrile moiety, for detecting the SO_2 and ClO^- in living cells and in vivo. MPIBA could report SO_2 and ClO^- with two reaction sites via the respective mechanism of nucleophilic addition and oxidation, resulting in the remarkable shift of fluorescent emission from 625 nm, respectively to 410 nm and 500 nm. These excellent properties provided the dual-ratiometric quantifications for SO_2 and NaClO, thereby ensuring the accurate calibration for biological analysis. With MPIBA, the ultrafast response (SO_2: < 60 seconds; ClO^-: within sec) and high sensitivity (detection limits: SO_2: 3.5 nM; ClO^-: 12.5 nM) were achieved. MPIBA was successfully applied to quantify the SO_2 and endogenous ClO^- in HeLa cells, Raw 264.7 cells. Moreover, the dynamics of SO_2 and endogenous ClO^- in zebrafish were visualized with MPIBA. Notably, the probe MPIBA can successively respond to SO_2 and ClO^-, which allowed a significant exploration on the dichotomous role of SO_2 under the ClO^- induced oxidative stress in HeLa cells.

2. Materials and methods

2.1. Synthesis of probe MPIBA

2.1.1. 4-(1H-phenanthro[9,10-d]imidazol-2-yl)benzaldehyde (PIB).

To a solution of glacial acetic acid (25 mL) in 50-mL round-bottom flask, 1,4-phthalaldehyde (600 mg, 4.5 mmol), 9,10-phenanthroquinone (310 mg, 1.5 mmol) and ammonium acetate (2.15 g, 30 mmol) were added. The mixture was heated to reflux for 30 min and then cooled to room temperature. The precipitate was collected by filtration, washed with acetate acid, and further purified by column chromatography on silica gel using hexane/ethyl acetate (v/v = 3:1). The yellow solid PIB was obtained (395.9 mg, 79.3%). ^{1}H NMR (DMSO-d6, 500MHz), δ (ppm): 10.141 (s,1H), 8.86 (d, J =8.5Hz, 2H), 8.62 (d, J = 4.5 Hz, 2H), 8.15 (q, J = 8.5Hz, 4H), 7.79 (q, J = 7.5 Hz, 2H), 7.68 (d, J = 7.0 Hz, 2H),), 2.953 (s, N-H, 1H). ^{13}C NMR (DMSO-d6, 125MHz), δ (ppm): (193.42, 151.33, 130.75, 130.20, 127.91, 127.71, 126.97, 126.22, 125.98, 124.94, 124.10, 122.35, 121.97.MS m/z calcd for $C_{22}H_{14}N_2O$ 322.37 $[M+H]^+$ found 322.8.

2.1.2. 4-(1-methyl-1H-phenanthro[9,10-d]imidazol-2-yl) benzaldehyde (MPIB)

To a solution of anhydrous acetonitrile (15 mL) in a 50-mL round-bottom flask, compound PIB (336 mg, 1.0 mmol), K_2CO_3 (150 mg, 1.1 mmol) and then CH_3I solution of (1.5 mmol in 15mL acetonitrile) were added dropwise in sequence with vigorous stirring. The mixture was stirred at room temperature for another 1 h, and filtrated to remove K_2CO_3. The obtained solution was reduced under vacuum at 60℃. The crude product was purified by column chromatography on silica gel using hexane/ethyl acetate (v/v 10:1) as eluent. A bright yellow solid of MPIB was obtained (280 mg, 80.5%). ^{1}H NMR (DMSO-d_6, 500 MHz), δ (ppm): 10.10 (s, 1H), 8.90 (d, J = 8.4 Hz, 1H), 8.86 (d, J = 8.4 Hz, 1H), 8.63 (d, J = 7.6 Hz, 1H), 8.57 (d, J = 7.6 Hz, 1H), 8.53 (d, J = 8.4 Hz, 2H), 8.14 (d, J = 8.4 Hz,

2H), 7.77 (d, J = 6.5 Hz, 2H), 7.67 (d, J = 7.5 Hz, 2H), 4.52 (s, 3H). ^{13}C NMR (DMSO-d_6, 125 MHz), δ(ppm): 193.37, 151.22, 130.75, 130.19, 127.87, 127.68, 126.16, 125.92, 124.98, 124.14, 123.53, 122.35, 122.01. MS, *m/z*, calcd for $C_{23}H_{16}N_2O$ 336.1 $[M+H]^+$, found. 336.5.

2.1.3. Synthesis of probe MPIBA

To a solution of compound MPIB (176 mg, 0.5 mmol, in 10 mL of pyridine) in a 50-mL round bottom flask, a solution of malononitrile (0.05 mL, 0.8 mmol, in 5 mL of pyridine) was rapidly added with vigorous stirring. The mixture was heated at reflux for 30 min, and then cooled to room temperature. The precipitate solid was collected by filtration, and the crude product was purified by silica column chromatography (hexane/ethyl acetate, v/v, 5:1) to obtain the probe MPIBA (red solid, 158 mg, 78.3%) (Figure S1). ^{1}H NMR (DMSO-d_6, 500 MHz), δ (ppm): 9.0 (d, J = 8.5 Hz, 1H), 8.89 (d, J = 8.5 Hz, 1H), 8.66 (d, J = 5.0 Hz, 1H), 8.62 (d, J = 5.0 Hz, 1H), 8.59 (q, J = 10 Hz, 2H), 8.18 (s, 1H), 7.79 (q, J = 14Hz, 2H), 7.74 (q, J = 11.5 Hz, 2H), 7.70 (q, J=15Hz,H) 7.44 (q, J=14Hz, H), 4.36 (s, 3H, N-CH_3).^{13}C NMR (DMSO-d_6, 125 MHz), δ (ppm): 161.01, 150.98, 137.47, 131.24, , 130.74, 127.90, 127.72, 126.24,125.00, 122.36, 122.07, 113.74, 82.53, 36.90. MS m/z calcd for $C_{26}H_{16}N_4$ 384.1, $[M+H]^+$ found 384.8.

2.2. Cells culture and imaging

HeLa cells and Raw 264.7 cells were obtained from the Committee on Type Culture Collection of Chinese Academy of Sciences (Shanghai, China), and were respectively incubated in DMEM medium and 1640 medium supplemented with 10% Fetal Bovine Serum (FBS, Invitrogen) at 37°C in a humidified incubator containing 5% CO_2 gas. Before imaging, cells were placed at 25-Petri dishes and allowed to adhere for 24 hours. Then, the cells were washed with DMEM medium and 1640 medium, and then incubated for 30 min at 37°C using MPIBA (5μM), respectively. Next, living cells were,

respectively, incubated with $NaHSO_3$ (0, 7.5, 15, 22.5 and 30 μM) and NaClO (0, 7.5, 15, 22.5 and 30 μM) (37 °C, 30 min, 5% CO_2) to establish the linear calibration for quantification.

To image the intracellular SO_2, HeLa cells were incubated with probe MPIBA (5μM) for 30 minutes and were then treated with *N*-benzyl-2,4-dini-trophenylsulfonamide (BTSA) (Supporting Information, Fig.S2) at 37°C for 60 min. To image the endogenous ClO^-, Raw 264.7 cells were incubated with MPIBA (5μM) for 30 min and were then incubated with LPS (1μgmL^{-1}) and PMA (1μgmL^{-1}) for 60 min at 37 °C. The tested cells were washed with DMEM medium or 1640 medium. Fluorescence imaging was performed by a confocal laser scanning microscope (Japan Olympus Co., Ltd) with an objective lens (×40).

2.3. Fluorescence imaging in zebrafish

In this study, zebrafishes were provided by HuanTe biological corporation (Hangzhou, China). All animal experiments were performed in full compliance with international ethical guidelines. Zebrafishes were incubated in E3 media (15 mM NaCl, 0.5 mM KCl, 1 mM $MgSO_4$, 1 mM $CaCl_2$, 0.15 mM KH_2PO_4, 0.05 mM Na_2HPO_4 and 0.7 mM $NaHCO_3$; pH 7.5) containing 5 μM MPIBA probe at 28°C for 1h, and then, the residual probe was washed by E3 media. To image the HSO_3^- in vivo, zebrafish larvae (three-days) were put into a 50 mm Petri dish filled with E3 media containing BTSA for 1~5 h. To image the endogenous ClO^-, zebrafish larvae (three-days) were put into a 50 mm Petri dish filled with E3 media containing 1 μg· mL^{-1} of LPS and PMA for 3~12 h. Fluorescence imaging was subsequently carried out by a confocal laser scanning microscope (Japan Olympus Co., Ltd) with an objective lens (×10).

2.4. Cross-Talk experiment for SO_2/ClO^- in HeLa cells

To explore the dichotomous roles of the intracellular SO_2, the cross-talk experiment of SO_2/ClO^- was

performed. HeLa cells were incubated in DMEM medium that contained 5μM of MPIBA for 30 min, and then, the BTSA was added to generate the SO_2. Then, cells were further incubated by MPO, H_2O_2 and NaCl for another 1h. As a control experiment, cells pretreated with probe were directly stimulated by MPO, H_2O_2 and NaCl for 1h. The whole process was followed by confocal laser scanning microscope (Japan Olympus Co., Ltd) with an objective lens (×10) and the flow cytometry to report the homeostasis of SO_2/ClO^- and the apoptosis rate.

3. Results and discussion

3.1. Design strategy for probe MPIBA

In our previous studies, phenanthroimidazole was used to synthesize fluorescent probes for labeling, exhibiting high fluorescence intensity and good photostability[31]. In this work, to extend the emission wavelength, we designed a parent fluorophore,4-(1-methyl-1H-phenanthro[9,10-d]-imidazol-2-yl) benzaldehyde (MPIB) (Scheme 1), based on the phenanthroimidazole. To achieve the large Stokes Shift, malononitrile was equipped to the fluorophore MPIB. The obtained probe MPIBA was characterized by NMR and ESI-MS (Supporting Information, Fig. S1). Experiences let us expect that such a design strategy may endow many attractive advantages to the probe MPIBA [32-35]. First, an extended π-electronic conjugation system in MPIBA can ensure the long emission and large Stokes Shift (Ex= 440 nm, Em=625 nm); Second, the strong electron-withdrawing group of malononitrile will allow the double bond carbon atom more easily attacked by nucleophile HSO_3^- thereby resulting in a blocked π-conjugation system in the product DMPIA, which may lead to the large shift of fluorescence emission; Third, the malononitrile-induced C=C bond can be oxidized by ClO^-, forming the aldehyde group conjugated product MPIB, which will lead to the relatively small shift of fluorescence emission;

Scheme 1.

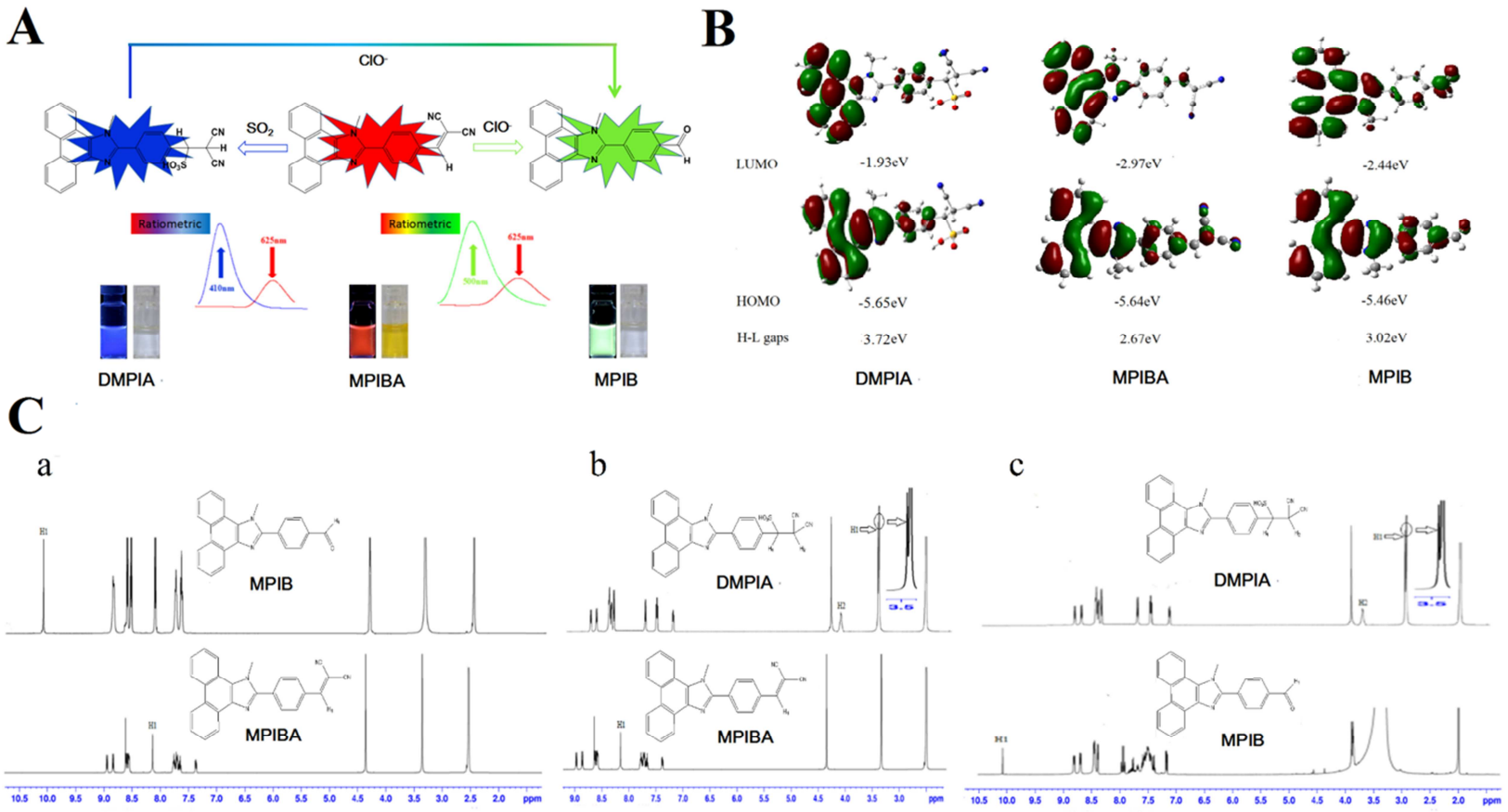
A
ClO⁻
SO2
ClO⁻
Ratiometric
625nm
410nm
Ratiometric
625nm
500nm
DMPIA
MPIBA
MPIB
B
LUMO
-1.93eV
-2.97eV
-2.44eV
HOMO
-5.65eV
-5.64eV
-5.46eV
H-L gaps
3.72eV
2.67eV
3.02eV
DMPIA
MPIBA
MPIB
C
a
MPIB
MPIBA
b
DMPIA
MPIBA
c
DMPIA
MPIB
ppm

Fourth, there is the potential that DMPIA can be oxidized by ClO^- to MPIB, which may enable the successive detection of SO_2 and ClO^-. To justify the rationality of this design, the MS-monitoring and ^1H NMR titration was performed (Scheme 1). When sensing the SO_2, the probe MPIBA was found to be transformed to DMPIA, as evidenced by the collision-induced dissociation MS spectra $[MPIBA+HSO_3^-+H]^+$ at *m/z* 466.8 and $[MPIBA+NaHSO_3]$ at *m/z* 488.5 (Fig. S2-A). NMR titration of MPIBA by $NaHSO_3$ showed two new peaks at δ=4.16 ppm (H2) and δ= 3.46 ppm (H1) (Scheme 1), confirming the formation of DMPIA via the nucleophilic addition reaction. When sensing the ClO^-, the MS spectra $[MPIBA+H]^+$ at *m/z*336.5 (Fig. S2-B) indicated that the probe MPIBA was transformed to MPIB which was further identified by the signal shift of alkene proton from δ=8.14 ppm to 10.13 ppm (Scheme 1). In addition, to investigate the reaction of DMPIA with excess ClO^-, the successive NMR titration was carried out. The disappearance of 3.46 ppm (H1) and the occurrence of 10.13 ppm (H1) in NMR spectrum (Scheme 1) indicate that the DMPIA can be oxidized by ClO^- to the product MPIB. Therefore, the probe MPIBA proves to be rationally designed.

3.2. Optical response of MPIBA toward HSO_3^- and ClO^-

Initially, we investigated the sensing ability of MPIBA(Φ=0.34) to HSO_3^- in DMSO/PBS buffer solution (50/50, v：v, pH = 7.4, 20 mM) at ambient temperature. As could be seen from the UV absorption spectra (Fig. S3), the probe MPIBA exhibited a strong peak at 427 nm. Upon addition of HSO_3^-, the remarkable blue shift in absorption was observed (363 nm) with a well-defined isosbestic point (375 nm), implying the formation of one stable product. By plotting the absorption ratio (A_{363}/A_{427}) versus the concentration of HSO_3^-, a good linear relationship was obtained. From the fluorescence spectra in Fig. 1A, 1B, we observed, upon addition of HSO_3^-, the emission peak at 625 nm decreased and simultaneously the strong emission peak at 410 nm (indicating product DMPI, Φ=0.84) rose up, which allowed the ratiometric quantification of HSO_3^-(Fig. 1C). When sensing ClO^-, the absorption spectra (Fig. S4) showed the decrease at 427 nm and simultaneously the increase at 373 nm with an isosbestic point at 395 nm. Fluorescence spectra (Fig. 1D) showed that with the increase of NaClO, the product MPIB (Φ=0.64) presented the peak centered at 500 nm. Meanwhile, the fluorescence emission peak at 625 nm was gradually decreased. Thus, the fluorescence ratiometric quantification for ClO^- was also enabled. Moreover, we performed a fluorescence titration of DMPIA with NaClO to investigate whether the probe MPIBA could successively detect SO_2 and ClO^-. As shown in Fig.1F, with the addition of ClO^-, the fluorescence emission of DMPIA (410 nm) decreased

and meanwhile an emission peak at 500 nm (indicating MPIB) appeared and rose up. These findings demonstrated that the probe MPIBA could be used to detect the ClO^- in the presence of the SO_2. These excellent optical properties demonstrated that the probe MPIBA was expected to produce the desired optical response needed to monitor the SO_2 and ClO^-.

Fig.1. Optical properties

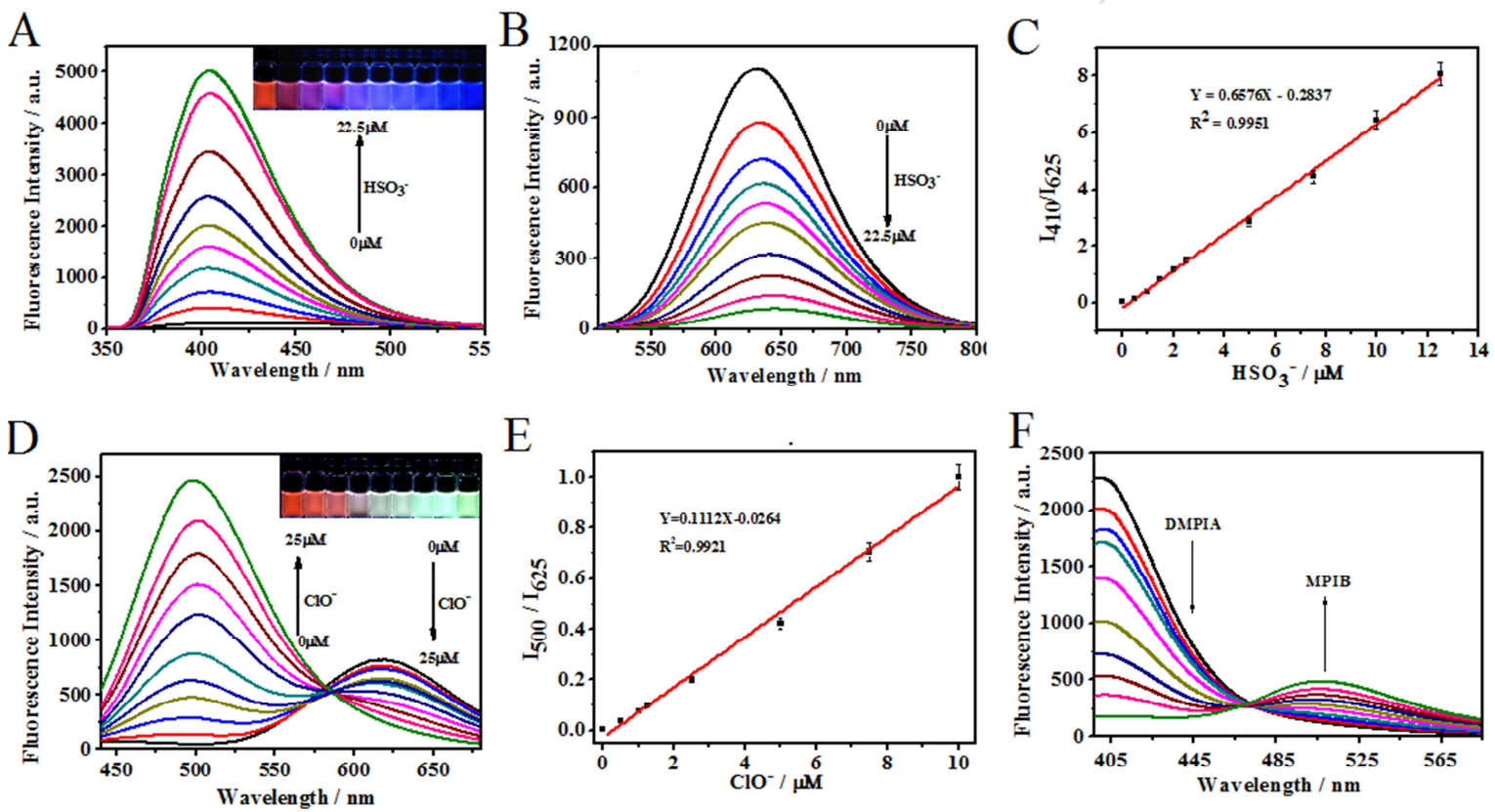

To understand the working mechanism of MPIBA, the HOMO (highest occupied molecular orbital) and the LUMO (lowest un-occupied molecular orbital) in MPIBA, DMPIA and MPIB were respectively calculated with density functional theory (DFT)[36-39](Scheme 1). As the result indicated, MPIBA showed the largest distribution of π-electrons in HOMO and the smallest energy gap between HOMO and LUMO among the three fluorescent compounds. Thus, an intramolecular charge-transfer (ICT) took place through the conjugated C=C double bond on MPIBA molecule, allowing this probe to release the red emission. In contrast, in DMPIA, the weakened delocalization of π-electrons with high LUMO was observed, resulting in the greatest energy gap, which accounted for the blue shift of emission of MPIBA in response to SO_2. In MPIB, the relatively smaller π-electrons and energy gap were consistent with its green emission, which should be attributed to the formation of the C=O from the oxidation of C=C by ClO^-.

3.3. Optimization of sensing conditions

First, time-dependent response was investigated (Fig. S5) and the fluorescence emission intensity at 625 nm was plotted as the reference. As time progressed, the probe MPIBA exhibited a steady fluorescence signal level. Upon addition of HSO_3^-, the intensity signal was dramatically and immediately decreased, reaching a plateau within 60 s (Fig S5, A). Similarly, a rapid response of MPIBA to NaClO was obtained within sec (Fig S5, B). These results indicated that the probe MPIBA provided the ultrafast response to both the two targets. Then, the pH-dependent fluorescence of MPIBA to HSO_3^- and ClO^- were respectively evaluated. As shown in Fig.S6, the pH 7.4 was beneficial to the strong fluorescent ratiometric response. Thus, the probe should be suitable for biological samples. In addition, temperature investigation (Fig.S7) showed that the satisfactory ratiometric responses of MPIBA to HSO_3^- and ClO^- could be obtained at the ambient temperature including the physiological temperature (37 ^oC). Therefore, the biological application of the developed probe can be expected.

3.4. Selectivity test

To evaluate the selectivity of MPIBA toward HSO_3^- and ClO^-, various biologically relevant species including anions (Cl^-, Br^-, I^-, CH_3COO^-, ClO_4^-, SO_4^{2-}, $H_2PO_4^-$, HS^-, $S_2O_3^{2-}$, SCN^-), metal ions (Na^+, K^+, Mg^{2+}, Fe^{3+}, Cd^{2+}, Co^{2+}, Ni^{2+}, Hg^{2+}, $Al3^+$, Mn^{2+}, Ag^+, Cu^{2+}, and Zn^{2+}), RSS (GSH, Cys, Hcy) and ROS/RNS (H_2O_2, $^{\cdot}OH$, TBHP, TBO^-, KO_2, $ONOO^-$, NO_2^-, NO_3^-, and NO), were investigated. Fluorescence intensity ratio (I_{410nm}/I_{625nm}) recorded in Fig. 2A~B showed that excessive metal ions, anions, and RSS, caused almost no interference to the HSO_3^-. Fig. 2C~D showed that no obvious

interference from the metal ions, anions, ROS and RNS was observed when sensing the ClO^-. Based on these investigations, it could be concluded that the developed MPIBA probe was able to selectively report both HSO_3^- and ClO^-.

Fig. 2. Selectivity experiments

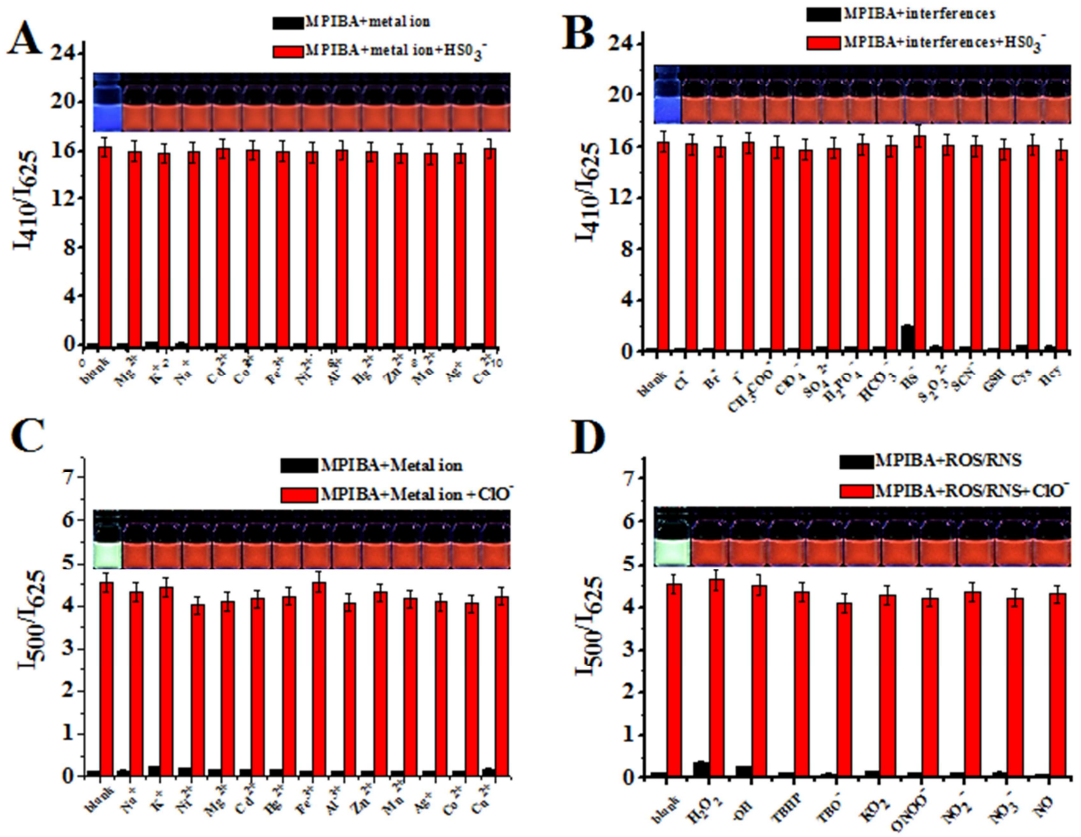

3.5. Calibration of SO_2/ClO^-

Calibration of SO_2 and ClO^- were separately investigated. As can be seen from Fig. 1, the two linear curves respectively for the quantification of ClO^- and HSO_3^- were established by the fluorescence ratios I_{410nm}/I_{625nm} and I_{500nm}/I_{625nm}, with the correlation coefficient of 0.9921 and 0.9951. Thus, the two analytes in the complicated biological media can be accurately quantified with this dual ratiometric probe MPIBA. Since the endogenous SO_2 and ClO^- was rather low, a rapid and sensitive detection was required. While, MPIBA provided the quite low detection limits for SO_2 (3.5 nM) and ClO^- (12.5 nM), which were comparable to the most sensitive chemical probes [40, 41]. Therefore, we thought, MPIBA exhibited the potential to detect SO_2 and ClO^- in cells or in vivo.

3.6. Penetration, photostability and cytotoxicity of MPIBA in living cells

The penetration and photostability of MPIBA in HeLa cell were evaluated. Dynamic fluorescence

imaging (Figure S 10) indicated that MPIBA could rapidly bring about the strong fluorescence ratiometric responses. These findings demonstrated the MPIBA quickly penetrated into the living cells and releases the strong fluorescence in responding to intracellular SO_2 and ClO^-. Then, the fluorescence intensity remained almost unchanged for 20 min, displaying the satisfactory photostability of MPIBA. Therefore the stable signals could be ensured when performing the intracellular monitoring with fluorescence image. Before the application, cytotoxicity of MPIBA to living cells was evaluated by MTT assay (Supporting Information). Fig. S8 showed that more than 90% cells still remained alive when 20 μM MPIBA probe was added for 24 h, demonstrating the low toxicity of MPIBA to the cultured cells under experimental conditions. Thus, MPIBA probe proved to be suitable for living cell imaging.

3.7. Ratiometric quantification of SO_2 in living cells

In view of these satisfactory properties of MPIBA, we set out to explore its intracellular ratiometric quantification for the two analytes. The ability of MPIBA for quantifying HSO_3^- was shown in Fig. 3A, where the living HeLa cells were incubated with MPIBA (5 μM) at 37 ^oC for 30 min in culture medium consisting of various concentrations of HSO_3^-. Clearly, the fluorescence intensity in red channel and blue channel showed respectively the decreasing and increasing trends in response to the increased level of HSO_3^-. These results provided the capability of this probe for ensuring the intracellular ratiometric quantifications of HSO_3^-. The pseudo colored images visualized the ratios variation of I_{blue}/I_{red} with the increasing HSO_3^-. Then the determination of SO_2 in living cells was carried out (Fig. 3B). The SO_2 donor, *N*-benzyl-2,4-dini-trophenylsulfonamide(BTSA)[42], was used to stimulate the SO_2 (HSO_3^-) with the intracellular thiol compounds such as Cys (Supporting Information, Fig. S9). It can be seen from Fig. 3B-a,b, upon addition of BTSA (25 μM), the remarkable fluorescence decrease in red channel and fluorescence increase in blue channel were observed. Accordingly, their ratiometric images were obtained, with which the ratios of I_{blue}/I_{red} were achieved. With the calibration curve (Fig. 1 C), the average content of SO_2 in the tested cells can be estimated. Taking into account of the slight background of probe as well as the spontaneously generated SO_2 in cells, we estimated the increased amount of SO_2 (stimulated by the donor BTSA) to be ~7.62 μM (standard deviation: SD=±0.2, n=11) (Fig. 3C). These findings let us conclude that this probe could be applied to the ratiometric quantification of the SO_2 in living cells. To justify this statement, the contrast experiments were carried out. The N-ethylmaleimide (NEM), an inhibitor for SO_2 formation by trapping intracellular Cys, was

added to the culture medium containing BTSA. Evidently from Fig 3B-c1, the strong fluorescence in red channel and the negligible fluorescence in blue channel were detected, which should be attributed to the inhibitive effect of NEM in HeLa cells. These results further confirmed the fact that probe MPIBA was successfully used to the ratiometric quantification of the SO_2 in living cells.

Fig. 3. Cells image for quantifying endogenous HSO_3^-

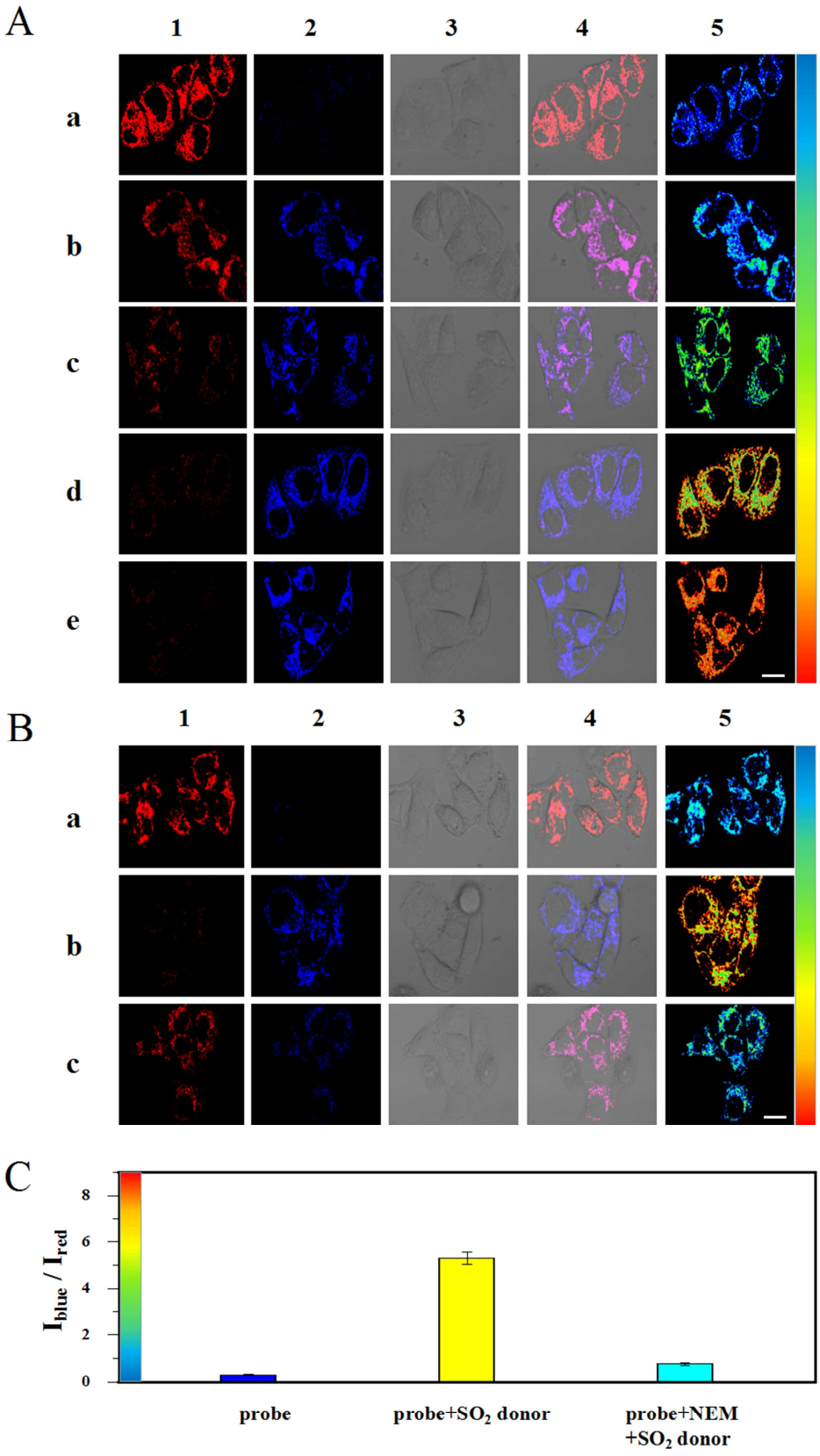
A
1
2
3
4
5
a
b
c
d
e
B
1
2
3
4
5
a
b
c
C
I_{blue} / I_{red}
0
2
4
6
8
probe
probe+SO_2 donor
probe+NEM
+SO_2 donor

3.8. Ratiometric quantification of endogenous ClO^- in living cells

Elevated levels of ClO^- may cause the oxidative damage to organisms. Therefore, the rapid and sensitive detection of endogenous ClO^- is significant. The fluorescence imaging of ClO^- in living Raw 264.7 cells using MPIBA probe was shown in Fig. 4. With the addition of NaClO (Fig 4A), the fluorescence intensity in red channel and blue channel showed respectively the decreasing and increasing trends in response to the increased level of ClO^-. These results indicated the ability of this probe for the intracellular ratiometric quantifications of ClO^-. The pseudo colored images presented the visualization of the fluorescence ratios (I_{green}/I_{red}) with the increasing amount of ClO^-. Then the determination of ClO^- in living cells was carried out (Fig. 4B). Lipopolysaccharide (LPS) and phorbol myristate acetate (PMA) were used as the stimulus to induce the generation of the endogenous ClO^- in Raw 264.7 cells[43]. As can be seen from Fig. 4B-a1, without stimulus, the cells showed mainly the red emission. In Fig. 4B-a2, the slight green emission implied the existence of spontaneous ClO^- in Raw 264.7 cells, which demonstrated the extraordinary sensitivity of the developed probe. Upon addition of PMA and LPS, the obvious decrease in red channel and increase in green channel were observed, which was consistent with the ratiometric response of MPIBA to ClO^- (Fig. 4B-b2). Based on the variation of the I_{green}/I_{red}, the intracellular increment of ClO^- was estimated to be 8.0 μM (standard deviation: SD=±0.2, n=11). Thus, this probe proved to be capable of quantifying the ClO^- living cells. To make sure that whether the ratio response was caused by the PMA-LPS-stimulated ClO^-, the contrast experiments were carried out. The intact Raw 264.7 cells were treated with 4-ABAH (50 μM) and probe MPIBA (5 μM) for 30 min, and then with LPS (1μgmL^{-1}) and PMA (1μgmL^{-1}) for 1 h (Fig. 4B-c), where the ABAH was used to reduce the intracellular ClO^- level through inhibiting the activity of MPO[44]. Comparing with the cells in Fig. 4B-b, the ABAH-inhibited cells showed the remarkable decrease of fluorescence in green channel but the increase of fluorescence in red channel (Fig.4B, c1-c2). This ratiometric response should be attributed to the reduced concentration of intracellular ClO^- due to the inhibitive effect of ABAH. Based on these experiments, we confirmed that MPIBA was capable of quantitative reporting the endogenous ClO^- in living cells.

Fig. 4. Cells image for exogenous and endogenous ClO^-

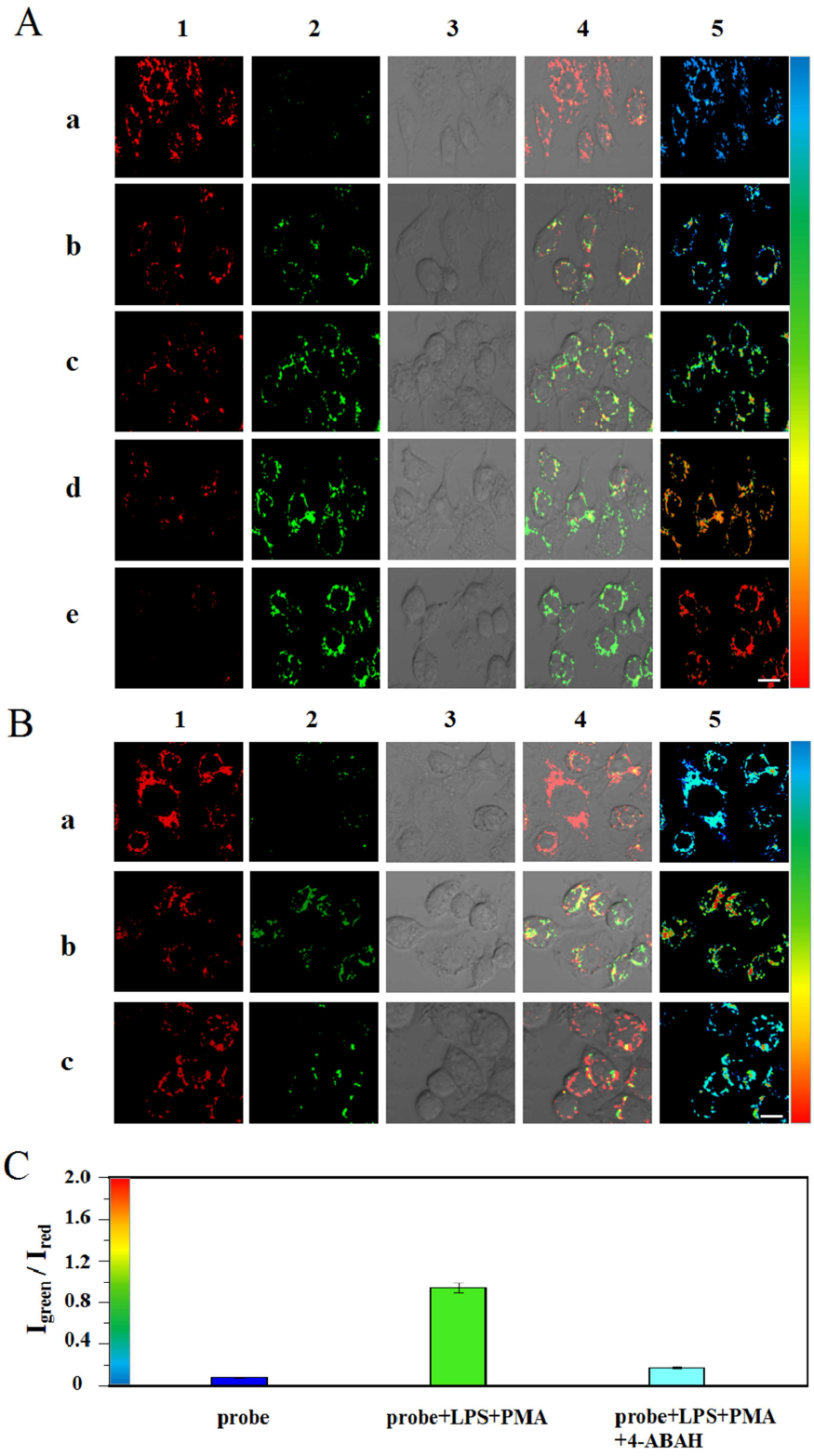
A
1
2
3
4
5
a
b
c
d
e
B
1
2
3
4
5
a
b
c
C
2.0
1.6
1.2
0.8
0.4
0
I_{green} / I_{red}
probe
probe+LPS+PMA
probe+LPS+PMA
+4-ABAH

*3.9. Imaging the dynamics of endogen*ous *ClO^- and SO_2 in zebrafish*

Zebrafish had around 87% homologous genes with human, and was widely adopted as a model organism of vertebrate biology[45]. In most cases, the experimental results obtained from zebrafish were also suitable for human body[46]. Therefore, zebrafish was selected as the animal mode in this work to evaluate the potential of MPIBA for imaging SO_2 and ClO^- in vivo. Up to date, little is known about the SO_2 dynamics in zebrafish, probably due to the lack of the suitable SO_2 probe. Therefore, we focused our initial efforts on monitoring the BTSA-induced SO_2 release in zebrafish. As could be seen from Fig. 5A-a, without BTSA, the zebrafish showed only the red emission, indicating the spontaneous SO_2 was too low to be detected under the experiment conditions. Upon addition of BTSA, the red emission began to decrease and correspondingly, the blue emission began to appear and increased in the next 1 to 5 h (Fig. 5A-b~c~d). This observation demonstrated that the SO_2 induced by BTSA in zebrafish was successfully detected by us. Then, to investigate whether the detected SO_2 was produced by the reaction of BTSA with Cys in vivo, we carried out the control experiments. First, we used the culture medium containing 1 mM NEM and BTSA to treat the zebrafish for 5 h. Then the obtained zebrafish was incubated with probe MPIBA for 1 h. As the result of this control experiment, Fig. 5A-e showed the strong fluorescence in red channel, which in turn confirmed that it was the BTSA induced SO_2 that triggered the fluorescence response of MPIBA. To the best of our knowledge, these results demonstrated the first use of fluorescence probe for imaging SO_2 in zebrafish, thus providing the opportunity for the new investigations of whole-organism analysis.

On the other hand, MPIBA was used to image the endogenous ClO^- in zebrafish. First, the MPIBA treated zebrafish showed only the red emission (Fig. 5B-a). Then, to the above medium, the LPS (1 μgmL^{-1}) and PMA (1 μgmL^{-1}) were added, and the fluorescence images were collected at 3 h, 6 h, and 12 h. As can be seen from Fig. 5B-b~c~d, the gradual increase of green emission and decrease of red emission were observed, suggesting the elevated levels of endogenous ClO^- in zebrafish. Next, ABAH was used to inhibit the generation of ClO^-. As expected, the Fig. 5B-e showed the strong red fluorescence but the rather weak green fluorescence. These findings demonstrated that MPIBA probe possessed the ability for imaging the endogenous ClO^- zebrafish.

Fig. 5. Imaging HSO_3^- and endogenous ClO^- in Zebrafish

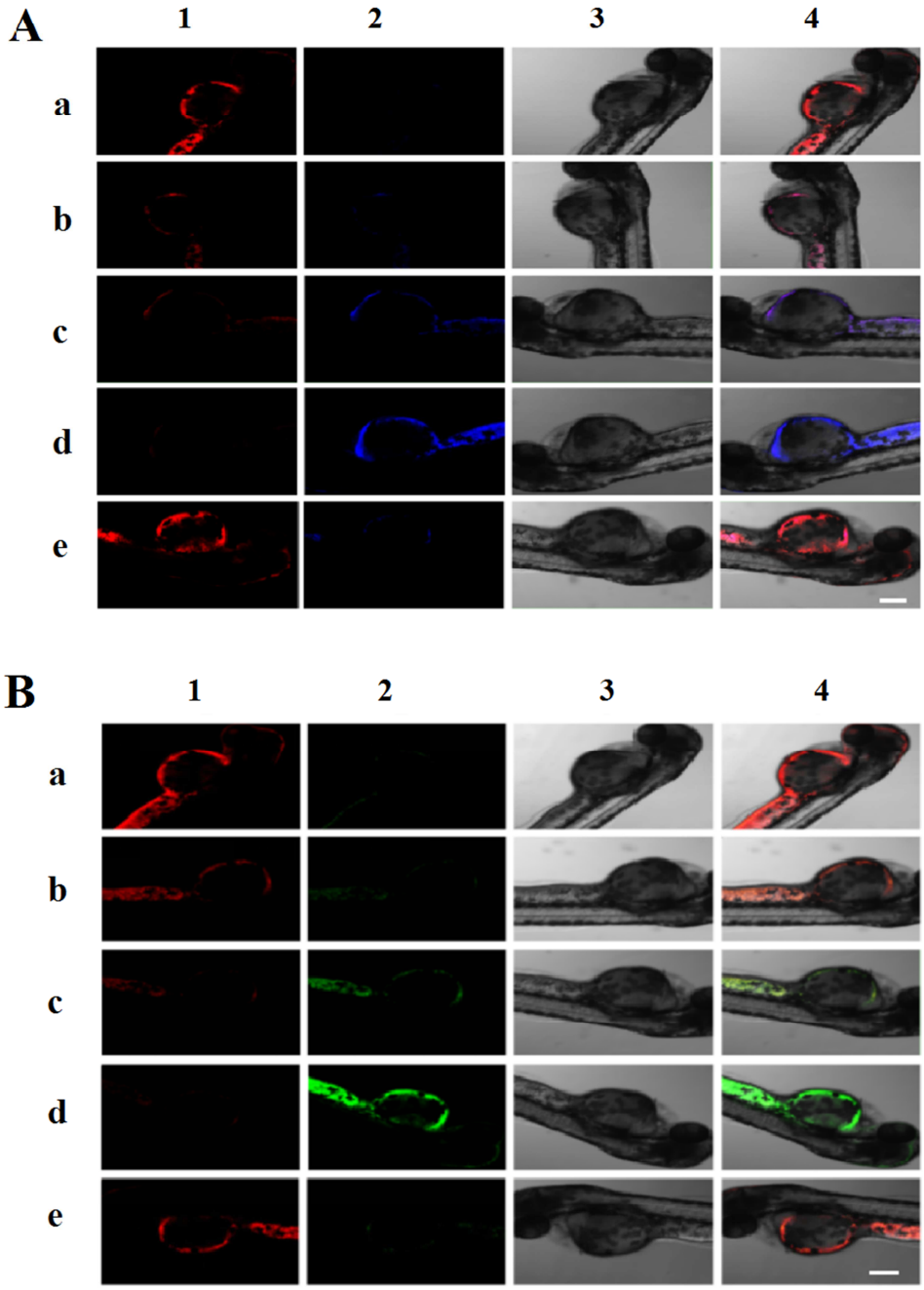

3.10. Cross-Talk influence of SO_2 and ClO^- to cells apoptosis

Above results exhibit the robust applicability of the probe MPIBA. Nevertheless, there is still the uncertain information about the dichotomous role of SO_2. As a signaling molecule, endogenous SO_2 can be produced by sulphur-containing amino acids, so as to increase the anti-oxidative capacity to a certain degree [47, 48]. However, SO_2 may also cause the occurrence and the progression of some oxidative injury in organs, which is always accompanied by the change of antioxidant status[16].

Therefore, further work is required to understand the dual role of SO_2. On the other hand, increasing evidences suggest that oxidative stress can be induced by ClO^- that was produced in presence of abnormal levels of MPO, which participated in the pathogenesis of diseases including cancer, cardiovascular diseases, and tissue inflammation[49-51]. As one of the most powerful oxidants, intracellular ClO^- may induce the apoptosis of cell. Considering the comprehensive influence of ClO^- together with SO_2 on cells, we reason that, SO_2 itself may cause the oxidative injury (such as apoptosis) to cells whereas in presence of ClO^-, SO_2 may resist the oxidative influence of ClO^- on cells. Consequently, a cross-talk effect of SO_2/ClO^- on intracellular cells can be expected, which is of great significance to the exploration of the dichotomous role of SO_2. Besides, exploring the cross-talk effect will contribute to the further investigation of the antioxidant defense mechanisms, the suppression of oxidative stress, as well as the cell apoptosis and autophagy[49, 52].

In present work, we monitored the homeostasis between SO_2 and ClO^- in HeLa cells and meanwhile, evaluated the influence of SO_2 and ClO^- to cell apoptosis. First of all, we investigated the applicability of MPIBA for reporting ClO^- in HeLa cells. Considering that ClO^- in HeLa cell could be produced with hydrogen peroxide and chloride ions via a myeloperoxidase (MPO)catalyzed reaction[3], the fluorescence imaging of ClO^- using

Fig. 6. Confocal fluorescence images and apoptosis analysis

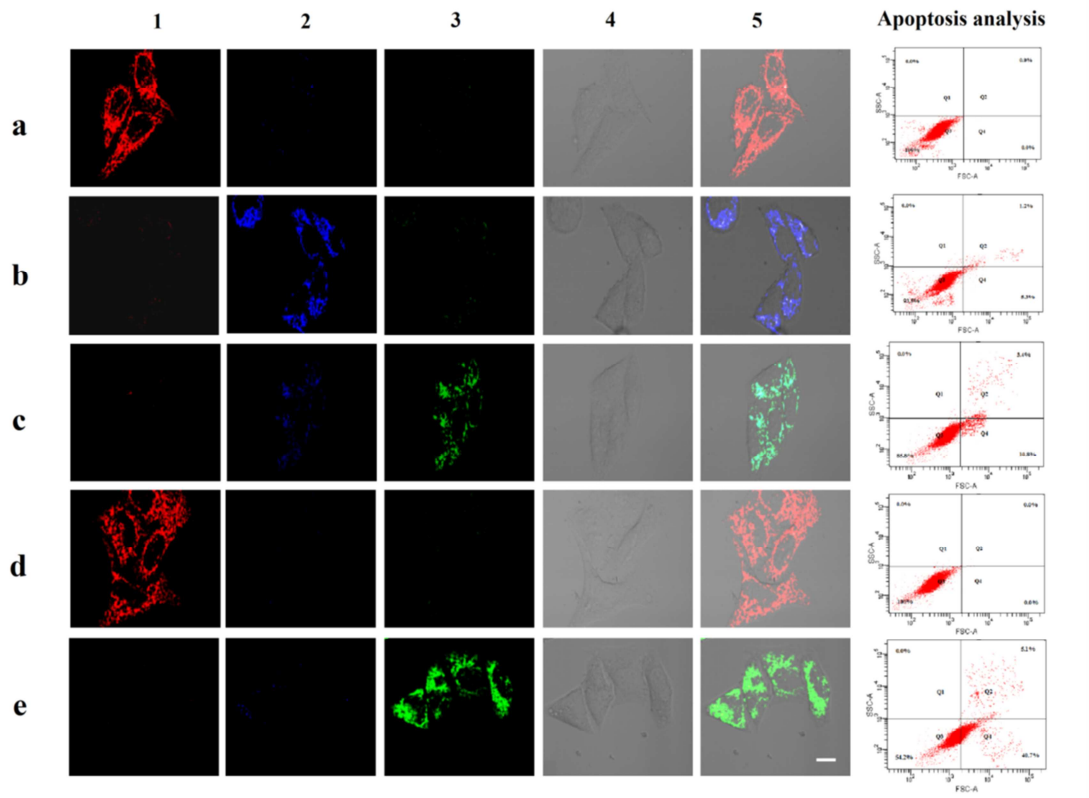

MPIBA probe in living HeLa cell was designed in Fig.S11. A set of systematic experiments including the non-stimulating experiment (Fig.S11a), MPO-H_2O_2-stimulating experiment (Fig. S11b), ABAH inhibiting experiment (Fig. S11c) and re-addition experiment (Fig. S11d), demonstrated the probe MPIBA was able to report ClO^- in HeLa cells. Thus, we set out to explore the intracellular cross-talk effect of SO_2 and ClO^-. As shown in Fig. 6, all parallel groups were pre-incubated with MPIBA (5 μM) for 30 min and washed three times with DMEM before imaging. As the control, the cells in Fig. 6a exhibited only red emission and the apoptosis rate in this control group was almost 0.0%. The treatment of HeLa cells with BTSA for 30 min would trigger the SO_2 burst. As expected, the blue emission in Fig. 6b was observed, indicating the elevated level of intracellular SO_2, The apoptosis rate of 6.5% implied the injurious effect of the excessive SO_2 in Hela cells. While, under the oxidative stress, the excessive reactive oxygen species would further oxidize the intracellular SO_2. Thus, the ClO^- could serve to induce the oxidative stress needed in this experiment. The treatment of HeLa cells with MPO (0.01 Unit), H_2O_2 (100 μM) and NaCl (500 mM) for 1 h would induce the rising level of ClO^-. As shown in Fig. 6c, the green emission appeared and the blue emission became weakened. These phenomena indicated the decrease of SO_2 and the increase of ClO^-. Meanwhile, the apoptosis rate increased up to 14.2%, which was consistent with the fact that ClO^- induced oxidative stress promoted the apoptosis of cells. As a control experiment, the HeLa cells in parallel groups (Fig. 6d) were treated directly with the

MPO (0.01 Unit), H_2O_2 (100 μM) and NaCl (500 mM) for 1 h (Fig. 6e). Results showed that the intracellular ClO^- level was high and accordingly the apoptosis rate was up to 45.8%。This finding confirmed that the ClO^- caused the more serious injury to cells without the stimulation of SO_2 (Fig. 6c), which in turn reflected the protective role of SO_2. To the best of our knowledge, this is the first time that the dual role (cell damage and cytoprotection) of intracellular SO_2, is visualized by the fluorescence imaging.

4. Conclusion

In summary, we have developed a dual-response fluorescent probe MPIBA for the respective or successive ratiometric quantification of SO_2 and ClO^- in cells and in vivo. MPIBA features the large Stokes shift, large absorbance/emission shift, ultrafast response, high sensitivity, dual-ratiometric-quantification and robust applicability, which demonstrates this probe a very attractive candidate for biological monitoring. Fluorescence confocal microscopic imaging for the RAW264.7 cells illustrates that this probe can be applied to quantify the burst of ClO^-. HeLa cells fluorescence imaging illustrates the quantification of the intracellular SO_2. Application of MPIBA in zebrafish indicates its ability to visualize the dynamic of SO_2 and ClO^- in vivo. Finally, we successfully apply the probe to detect the homeostasis of SO_2/ClO^- and the corresponding bio-influence in HeLa cells. Results have elucidated the dichotomous effect of intracellular SO_2 under the oxidative stress, wherein the SO_2 can exert both oxidative and anti-oxidative effects to cells. We envision that such a desirable probe can provide invaluable insights into how SO_2/ClO^- works in extensive biological systems.

Acknowledgments

This work was supported by the National Natural Science Foundation of China (Nos: 21475074, 21403123, 21375075, 31301595, 21402106, 21475075, 21275089, 21405093, 21405094, 81303179, 21305076), the Open Funds of the Shandong Province Key Laboratory of Detection Technology for Tumor Markers (KLDTTM2015-6), the Opening Foundation of Shandong Provincial Key Laboratory of Detection Technology for Tumor Markers (KLDTTM2015-9) and the Taishan Scholar Foundation of Shandong Province, P. R. China.

References

[1] C.-H. Chang, E.L. Pearce, Emerging concepts of T cell metabolism as a target of immunotherapy, Nat Immunol 17 (4) (2016) 364-368.

[2] X. Chen, X. Tian, I. Shin, J. Yoon, Fluorescent and luminescent probes for detection of reactive oxygen and nitrogen species, Chem Soc Rev 40 (9) (2011) 4783.

[3] Y.W. Yap, M. Whiteman, N.S. Cheung, Chlorinative stress: An under appreciated mediator of neurodegeneration?, Cell Signal 19 (2) (2007) 219-228.

[4] L.J. Hazell, L. Arnold, D. Flowers, G. Waeg, E. Malle, R. Stocker, Presence of hypochlorite-modified proteins in human atherosclerotic lesions, J Clin Invest 97 (6) (1996) 1535-44.

[5] J.K. Andersen, Oxidative stress in neurodegeneration: cause or consequence?, Nat Med 10 Suppl (2004) S18-25.

[6] T. Kaur, K.L. Khanduja, R. Gupta, N.M. Gupta, K. Vaiphei, Changes in antioxidant defense status in response to cisplatin and 5-FU in esophageal carcinoma, Dis Esophagus 21 (2) (2008) 103-107.

[7] Y. Sun, J. Liu, J. Zhang, T. Yang, W. Guo, Fluorescent probe for biological gas SO2 derivatives bisulfite and sulfite, Chem Commun 49 (26) (2013) 2637-2639.

[8] J. Li, Z. Meng, The role of sulfur dioxide as an endogenous gaseous vasoactive factor in synergy with nitric oxide, Nitric Oxide 20 (3) (2009) 166-174.

[9] J.L. Wallace, R. Wang, Hydrogen sulfide-based therapeutics: exploiting a unique but ubiquitous gasotransmitter, Nat Rev Drug Discov 14 (5) (2015) 329-345.

[10] H. Li, L. Sun, E.L. de Carvalho, X. Li, X. Lv, G.J. Khan, H. Semukunzi, S. Yuan, S. Lin, DT-13, a saponin monomer of dwarf lilyturf tuber, induces autophagy and potentiates anti-cancer effect of nutrient deprivation, Eur J Pharmacol 781 (2016) 164-172.

[11] D.I. Pattison, M.J. Davies, Evidence for Rapid Inter- and Intramolecular Chlorine Transfer Reactions of Histamine and Carnosine Chloramines: Implications for the Prevention of Hypochlorous-Acid-Mediated Damage, Biochemistry 45 (26) (2006) 8152-8162.

[12] J.S. Gujral, A. Farhood, M.L. Bajt, H. Jaeschke, Neutrophils aggravate acute liver injury during obstructive cholestasis in bile duct-ligated mice, Hepatology 38 (2) (2003) 355-363.

[13] J.S. Gujral, J.A. Hinson, A. Farhood, H. Jaeschke, NADPH oxidase-derived oxidant stress is critical for neutrophil cytotoxicity during endotoxemia, Am Jphysiol-Gastrl 287 (1) (2004) G243-52.

[14] T. Hasegawa, E. Malle, A. Farhood, H. Jaeschke, Generation of hypochlorite-modified proteins by neutrophils during ischemia-reperfusion injury in rat liver: attenuation by ischemic preconditioning, Am Jphysiol-Gastrl 289 (4) (2005) 760-7.

[15] S. Sugiyama, K. Kugiyama, M. Aikawa, S. Nakamura, H. Ogawa, P. Libby, Hypochlorous acid, a macrophage product, induces endothelial apoptosis and tissue factor expression, Arterioscl Throm Vas 24 (2004) 1309.

[16] Z. Meng, Oxidative damage of sulfur dioxide on various organs of mice: sulfur dioxide is a systemic oxidative damage agent, Inhal Toxicol 15 (2) (2003) 181.

[17] A. Kubo, H. Saji, K. Tanaka, N. Kondo, Expression of arabidopsis cytosolic ascorbate peroxidase gene in response to ozone or sulfur dioxide, Plant Mol Biol 29 (3) (1995) 479-489.

[18] Q. Zhang, Z. Zhu, Y. Zheng, J. Cheng, N. Zhang, Y.T. Long, J. Zheng, X. Qian, Y. Yang, A three-channel fluorescent probe that distinguishes peroxynitrite from hypochlorite, J Am Chem Soc 134 (45) (2012) 18479-82.

[19] X. Shen, E.A. Peter, S. Bir, R. Wang, C.G. Kevil, Analytical measurement of discrete hydrogen sulfide pools in biological specimens, Free Radical Biology and Medicine 52 (11–12) 2276-2283.

[20] A. Isaac, J. Davis, C. Livingstone, A.J. Wain, R.G. Compton, Electroanalytical methods for the determination of sulfite in food and beverages, Trac-Trend Aanal. Chem. 25 (6) (2006) 589-598.

[21] M. Koch, R. Köppen, D. Siegel, A. Witt, I. Nehls, Determination of total sulfite in wine by ion chromatography after in-sample oxidation, J Agr Food Chem 58 (17) (2010) 9463-9467.

[22] L. Yuan, L. Wang, B.K. Agrawalla, S.J. Park, H. Zhu, B. Sivaraman, J. Peng, Q.H. Xu, Y.T. Chang, Development of targetable two-photon fluorescent probes to image hypochlorous Acid in mitochondria and lysosome in live cell and inflamed mouse model, J Am Chem Soc 137 (18) (2015) 5930-8.

[23] R. Zhang, J. Zhao, G. Han, Z. Liu, C. Liu, C. Zhang, B. Liu, C. Jiang, R. Liu, T. Zhao, M.Y. Han, Z. Zhang, Real-Time Discrimination and Versatile Profiling of Spontaneous Reactive Oxygen Species in Living Organisms with a Single Fluorescent Probe, J Am Chem Soc 138 (11) (2016) 3769-78.

[24] Q. Xu, C.H. Heo, J.A. Kim, H.S. Lee, Y. Hu, D. Kim, K.M. Swamy, G. Kim, S.J. Nam, H.M. Kim, J. Yoon, A Selective Imidazoline-2-thione-Bearing Two-Photon Fluorescent Probe for Hypochlorous Acid in Mitochondria, Anal Chem 88 (12) (2016) 6615-20.

[25] Y. Zhang, L. Guan, H. Yu, Y. Yan, L. Du, Y. Liu, M. Sun, D. Huang, S. Wang, Reversible Fluorescent Probe for Selective Detection and Cell Imaging of Oxidative Stress Indicator Bisulfite, Anal Chem 88 (8) (2016) 4426-31.

[26] Y. Huang, F. Yu, J. Wang, L. Chen, Near-Infrared Fluorescence Probe for in Situ Detection of Superoxide Anion and Hydrogen Polysulfides in Mitochondrial Oxidative Stress, Anal Chem 88 (7) (2016) 4122-9.

[27] S.K. Bae, C.H. Heo, D.J. Choi, D. Sen, E.H. Joe, B.R. Cho, H.M. Kim, A ratiometric two-photon fluorescent probe reveals reduction in mitochondrial H2S production in Parkinson's disease gene knockout astrocytes, J Am Chem Soc 135 (26) (2013) 9915-23.

[28] H. Zhu, J. Fan, J. Wang, H. Mu, X. Peng, An "enhanced PET"-based fluorescent probe with ultrasensitivity for imaging basal and elesclomol-induced HClO in cancer cells, J Am Chem Soc 136 (37) (2014) 12820-3.

[29] M.H. Lee, J.S. Kim, J.L. Sessler, Small molecule-based ratiometric fluorescence probes for cations, anions, and biomolecules, Chem Soc Rev 44 (13) (2015) 4185-91.

[30] X. Chen, F. Wang, J.Y. Hyun, T. Wei, J. Qiang, X. Ren, I. Shin, J. Yoon, Recent progress in the development of fluorescent, luminescent and colorimetric probes for detection of reactive oxygen and nitrogen species, Chem Soc Rev 45 (10) (2016) 2976-3016.

[31] Z. Sun, J. You, C. Song, L. Xia, Identification and determination of carboxylic acids in food samples using 2-(2-(anthracen-10-yl)-1H-phenanthro[9,10-d]imidazol-1-yl)ethyl 4-methylbenzenesulfonate (APIETS) as labeling reagent by HPLC with FLD and APCI/MS, Talanta 85 (2) (2011) 1088-1099.

[32] Q. Fu, Z. Chen, X. Ma, G. Chen, Y. Liu, Z. Cao, F. Qu, D. Yang, X. Zhao, Z. Sun, Simultaneous absorbance-ratiometric, fluorimetric, and colorimetric analysis and biological imaging of α-ketoglutaric acid based on a special sensing mechanism, Sensors & Actuators B Chemical (2016).

[33] G. Chen, J. Liu, M. Liu, G. Li, Z. Sun, S. Zhang, C. Song, H. Wang, Y. Suo, J. You, Sensitive, accurate and rapid detection of trace aliphatic amines in environmental samples with ultrasonic-assisted derivatization microextraction using a new fluorescent reagent for high performance liquid chromatography, J Chromatogr A 1352 (2014) 8-19.

[34] J. Liu, M. Liu, X. Li, X. Lu, G. Chen, Z. Sun, G. Li, X. Zhao, S. Zhang, C. Song, Development of ultrasonic-assisted closed in-syringe extraction and derivatization for the determination of labile abietic acid and dehydroabietic acid in cosmetics, J Chromatogr A 1371 (2014) 20-29.

[35] M. Liu, G. Chen, H. Guo, B. Fan, J. Liu, Q. Fu, X. Li, X. Lu, X. Zhao, G. Li, Accurate Analysis and Evaluation of Acidic Plant Growth Regulators in Transgenic and Nontransgenic Edible Oils with Facile Microwave-Assisted Extraction-Derivatization, J Agr Food Chem 63 (36) (2015) 8058-67.

[36] Y. Liu, X. Yang, L. Liu, H. Wang, S. Bi, Mechanistic insight into water-modulated cycloisomerization of enynyl esters using an Au(I) catalyst, Dalton Trans 44 (12) (2015) 5354-5363.

[37] Y. Liu, G. Chen, H. Wang, S. Bi, D. Zhang, Theoretical Investigation of the Controlled Metathesis Reactions of Methylruthenium(II) Complexes with Terminal Acetylenes, Eur J Inorg Chem 2014 (15) (2014) 2502–2511.

[38] L. Liu, Y. Liu, B. Ling, S. Bi, Mechanistic investigation into Et 3 N C H activation and chemoselectivity by Pd-Catalyzed intramolecular heck reaction of N-Vinylacetamides, J Organomet Chem 827 (2017) 56-66.

[39] Y. Liu, Y. Tang, Y.-Y. Jiang, X. Zhang, P. Li, S. Bi, Mechanism and Origin of Et2Al(OEt)-Induced Chemoselectivity of Nickel-Catalyzed Three-Component Coupling of One Diketene and Two Alkynes, ACS Catalysis 7 (3) (2017) 1886-1896.

[40] W. Chen, Q. Fang, D. Yang, H. Zhang, X. Song, J. Foley, Selective, Highly Sensitive Fluorescent Probe for the Detection of Sulfur Dioxide Derivatives in Aqueous and Biological Environments, Anal Chem 87 (1) (2015) 609-16.

[41] J.J. Hu, N.K. Wong, M.Y. Lu, X. Chen, S. Ye, A.Q. Zhao, P. Gao, Y.T. Kao, J. Shen, D. Yang, HKOCl-3: a fluorescent hypochlorous acid probe for live-cell and in vivo imaging and quantitative application in flow cytometry and a 96-well microplate assay, Chem Sci 7 (1) (2016) 39-53.

[42] W. Xu, L.T. Chai, J. Peng, D. Su, L. Yuan, Y.T. Chang, A mitochondria-targeted ratiometric fluorescent probe to monitor endogenously generated sulfur dioxide derivatives in living cells, Biomaterials 56 (2015) 1-9.

[43] Q. Xu, C.H. Heo, J.A. Kim, H.S. Lee, Y. Hu, D. Kim, K.M. Swamy, G. Kim, S.J. Nam, H.M. Kim, A Selective Imidazoline-2-Thione-Bearing Two-Photon Fluorescent Probe for Hypochlorous Acid in Mitochondria, Anal Chem 88 (12) (2016).

[44] M. Fujihara, M. Muroi, K.I. Tanamoto, T. Suzuki, H. Azuma, H. Ikeda, Molecular mechanisms of macrophage activation and deactivation by lipopolysaccharide: roles of the receptor complex, Pharmacol Therapeut 100 (2) (2003) 171-194.

[45] Y. Liu, D. Li, Z. Yuan, Photoacoustic Tomography Imaging of the Adult Zebrafish by Using Unfocused and Focused High-Frequency Ultrasound Transducers, Applied Sciences 6 (12) (2016) 392.

[46] Y. Drabsch, Transforming growth factor-β signalling controls human breast cancer metastasis in a zebrafish xenograft model, Breast Cancer Res 15 (6) (2013) R106.

[47] T. Ubuka, S. Yuasa, J. Ohta, N. Masuoka, K. Yao, M. Kinuta, Formation of sulfate from L-cysteine in rat liver mitochondria, Acta Med Okayama 44 (2) (1990) 55-64.

[48] L. Luo, S. Chen, H. Jin, C. Tang, J. Du, Endogenous generation of sulfur dioxide in rat tissues, Biochem Biophys Res Commun 415 (1) (2011) 61-67.

[49] J. Shepherd, S.A. Hilderbrand, P. Waterman, J.W. Heinecke, R. Weissleder, P. Libby, A Fluorescent Probe for the Detection of Myeloperoxidase Activity in Atherosclerosis-Associated Macrophages, Chem Biol 14 (11) (2007) 1221.

[50] B. Halliwell, Oxidative stress and cancer: have we moved forward?, Biochem J 401 (1) (2007) 1.

[51] S. Sugiyama, Y. Okada, G.K. Sukhova, R. Virmani, J.W. Heinecke, P. Libby, Macrophage Myeloperoxidase Regulation by Granulocyte Macrophage Colony-Stimulating Factor in Human Atherosclerosis and Implications in Acute Coronary Syndromes, Am J Pathol 158 (3) (2001) 879-891.

[52] H.H. Wu, T.Y. Hsiao, C.T. Chien, M.K. Lai, Ischemic conditioning by short periods of reperfusion attenuates renal ischemia/reperfusion induced apoptosis and autophagy in the rat, J Biomed Sci 16 (1) (2009) 1-10.

Figure Captions

Scheme 1. A: the proposed sensing strategy of probe MPIBA to SO_2 and ClO^- **B**: frontier molecular orbital plots of probe MPIBA, DMPIA and MPIB. Green and red shapes are corresponding to the different phases of the molecular wave functions for HOMO and LUMO orbitals. C-a: Partial ^1H NMR spectra of MPIBA in DMSO-d_6 and ^1H NMR spectra of MPIBA in the presence of NaClO in DMSO-d_6/D_2O; C-a: Partial ^1H NMR spectra of MPIBA and in the presence of $NaHSO_3$ in DMSO-d_6/D_2O, and C-c: partial ^1H NMR spectra of DMPIA in the presence of NaClO in DMSO-d_6/D_2O

Fig. 1. Fluorescence response of probe MPIBA (5 μM) to HSO_3^- and ClO^- were respectively investigated in DMSO/PBS buffer solution (50/50, v/v, pH = 7.4, 20 mM). (**A**): fluorescence response at 410 nm (ex=330 nm) to HSO_3^- (0 to 12.5 μM); (**B**): fluorescence response at 625 nm (ex=440 nm) to HSO_3^- (0 to 12.5 μM); (**C**): the linear curve established by fluorescence ratios (I_{410}/I_{625}) versus the concentrations of HSO_3^-; (**D**): the fluorescence response (ex=410 nm) of MPIBA to ClO^- (0 to 25 μM); (**E**): the linear curve established by fluorescence ratios (I_{500}/I_{625}) versus the concentrations of NaClO; (**F**): the fluorescence response of the DMPIA (see Scheme 1) to increased NaClO (0-50 μM) (ex=380 nm slits:10/10nm).

Fig. 2. (**A**) Fluorescence ratio response of probe MPIBA (5 μM) towards HSO_3^- (20 μM) in presence of metal ion (1 mM); (**B**) Fluorescence ratio response of MPIBA (5 μM) to HSO_3^- (20 μM) in presence of anions (1mM) and other biological thiols (0.5 mM) in DMSO/PBS buffer solution (50/50, v/v, pH = 7.4, 20 mM); (**C**) Fluorescence ratio response of MPIBA (5 μM) towards NaClO (20 μM) in presence of metal ion (1 mM); (**D**) Fluorescence ratio response of MPIBA (5 μM) towards NaClO (20 μM) in presence of various ROS and RNS (200 μM) in DMSO/PBS buffer solution (50/50, v/v, pH = 7.4, 20 mM).

Fig. 3. (A) Confocal fluorescence images for HeLa cells pretreated with probe MPIBA (5 μM) with addition of different levels of HSO_3^- (**a**: 0 μM, **b**: 7.5 μM, **c**: 15 μM, **d**: 22.5 μM, **e**: 30 μM) for 30 min. (B) Confocal fluorescence images for endogenously generated HSO_3^-. Intact Hela cells were incubated with MPIBA (5 μM) for 30 min (**a1**-**a5**) and then were incubated with N-benzyl-2,4-dini-trophenylsulfonamide (BTSA) for 1h (**b1**-**b5**); To get the control group, intact HeLa cells were treated with N-ethylmaleimide (NEM) (1mM) and probe MPIBA (5 μM) for 30 min, and then with 25 μM BTSA for 1 h (**c1**-**c5**). (C) The average fluorescence ratios collected from the images (B: a5: probe; b5: probe+ donor BTSA; c5: probe+NEM+BTSA). Error bars are ± SD, n=11. (1: red channel (λex=488 nm, λem=570–670 nm), 2: blue channel (λex=405 nm, λem =420–470nm), 3: bright-field, 4: overlap of (1), (2) and (3), 5: ratio imaging (I_{blue}/I_{red})). Scale bar: 20 μm.

Fig. 4. (A) Confocal fluorescence images for Raw264.7 cells pretreated with probe MPIBA (5 μM) and different levels of ClO^- (**a**: 0 μM, **b**: 7.5 μM, **c**: 15 μM, **d**: 22.5 μM, **e**: 30 μM) for 30 min. (B) Confocal fluorescence images for endogenous ClO^-. Intact cells were incubated with MPIBA (5 μM) for 30 min (**a1**-**a5**) and then were incubated with LPS (1 μgmL^{-1}) and PMA (1 μgmL^{-1}) for 1 h; To get the control group, intact Raw264.7 cells were treated with 4-ABAH (50 μM) and probe MPIBA (5 μM) for 30 min, and then with LPS (1μgmL^{-1}) and PMA (1μgmL^{-1}) for 1 h (**c1**-**c5**). (C) The average fluorescence ratios

collected from the images (B: a5: probe; b5: probe+LPS+PMA; c5: probe+LPS+PMA+4-ABAH**)**. Error bars are ± SD, n=11. (1: red channel (λex=488 nm, λem =570–670nm), 2: green channel (λex=405 nm, λem =470–570nm), 3: bright-field, 4: overlap of (1), (2), (3), 5: ratio imaging (I green/ I red)). Scale bar: 20 μm.

Fig. 5. (**A**) Fluorescence images of zebrafish larvae incubated with BTSA. The zebrafish was fed with the probe (5 μM) for 1h (**a1-a4**); the larva was pretreated with probe in E3 media for 60 min and was then incubated with BTSA for 1 h **(b1-b4**), 3h (**c1-c4**) or 5 h (**d1-d4**); To get control group, zebrafish was incubated with 1 mM N-ethylmaleimide (NEM) and BTSA (SO_2 donor) for 5 h, then further treated with probe MPIBA for 1h (**e1-e4**); Fluorescence images from **1** to **4** represent, **1**: red channel (λex=488 nm, λem =570–670nm), **2**: blue channel (λex=405 nm, λem =420–470nm), **3**: bright-field, **4**: overlap of (1), (2), (3). Scale bar: 200 μm. (**B**) Fluorescence images of zebrafish larvae that was treated with LPS (1 μgmL^{-1}) and PMA (1 μgmL^{-1}). The zebrafish was treated with probe (5 μM) for 1h (**a1-a4**); then, the larva was treated with LPS (1 μgmL^{-1}) and PMA (1 μgmL^{-1}) for 3 h (**b1-b4**), 5 h (**c1-c4**) and 12 h (**d1-d4**); To get control group, zebrafish were pretreated with 4-ABAH (50 μM) and LPS(1 μgmL^{-1}) and PMA (1 μgmL^{-1}) upon 12 h, then with probe for another 1 h (**e1-e4**); Fluorescence images **1** to **4** represent, **1**: red channel (λex=488 nm, λem =570–670nm), **2**: green channel (λex=405 nm, λem =470–570nm), **3**: bright-field, **4**: overlap of (1), (2), (3). Scale bar: 200 μm.

Fig. 6. Confocal microscopy images and apoptosis analysis for evaluating the bio-activities of intracellular SO_2, HeLa cells were incubated with MPIBA (5 μM) for 30 min (**a1-a5**) and then incubated with 50 μM BTSA for 60 min (**b1-b5**). Next, 0.01 Unit of MPO, 100 μM H_2O_2 and 500 mM NaCl was added to cells and the mixture was further incubated for 1h (**c1-c5**). To perform the control experiments, HeLa cells were incubated with probe MPIBA (5 μM) for 30 min (**d1-d5**) and then with the media consisting of 0.01 Unit of MPO, 100 μM H_2O_2 and 500 mM NaCl for 1h (**e1-e5**). (**1**: red channel (λex=488 nm, λem =570–670nm), **2**: blue channel (λex=405 nm, λem =420–470nm), **3**: green channel (λex=405 nm, λem =470–570nm) **4**: bright-field, **5**: overlap of (**1**), (**2**) and (**3**). Scale bar: 20μm. Apoptosis analysis: areas of Q1, Q2, Q3, Q4 were corresponding necrotic, late apoptosis, viable, and early apoptosis.

Graphic Abstract